Catalysis Today 151 (2010) 251–256

Contents lists available at ScienceDirect

Catalysis Today

journal homepage: www.elsevier.com/locate/cattod

Selective catalytic reduction of NO with NH_3 over Mn–Fe/USY under lean burn conditions

Qichun Lin [a,b], Junhua Li [a,*], Lei Ma [a], Jiming Hao [a]

[a] Department of Environmental Science and Engineering, Tsinghua University, Beijing 100084, China
[b] Ningbo Environmental Protection Bureau, Ningbo 315012, China

ARTICLE INFO

Article history:
Available online 20 February 2010

Keywords:
Selective catalytic reduction of NO with NH_3
Lean burn conditions
Mn/USY
Mn–Fe/USY

ABSTRACT

A series of catalysts of Mn/USY and Mn–Fe/USY prepared by impregnation were studied for selective catalytic reduction (SCR) of NO with NH_3 under lean burn conditions. The most active 10%Mn–8%Fe/USY catalyst nearly reached 100% NO conversion with the space velocity of 36,000 h^{-1} in the wide temperature range of 423–573 K. Both manganese and iron oxides dispersed well, no visible manganese or iron oxide phase was observed in X-ray powder diffraction (XRD) spectra. In addition, Mn and Fe oxides on Mn–Fe/USY catalyst, which were prepared by impregnation, were mainly formed MnO_2 and γ-Fe_2O_3 by X-ray photoelectron spectroscopy (XPS). Diffuse reflectance infrared Fourier transform spectroscopy (DRIFTS) results showed that Fe promoted NO oxidation and created more monodentate and bidentate nitrates adsorbed species on the catalyst surface. The addition of Fe enhanced the quantity and strength of the Brönsted and Lewis acid sites on the surface of 10%Mn–8%Fe/USY, which might promote the absorption of NH_3 to form active intermediate and increase the catalytic performance at low temperature. FT-IR spectra of chemisorbed pyridine (Py-IR) results also demonstrated the increase in acidity of 10%Mn–8%Fe/USY catalyst by Fe promotion effect.

1. Introduction

Nitrogen oxides (NO_x) emitted from automobiles and stationary sources are major cause for photochemical smog, acid rain and ozone depletion [1–4]. Removal of NO_x from the exhaust of lean burn and diesel engines is a major challenge to fulfill future restrictive standard emissions [5]. Selective catalytic reduction (SCR) of NO to N_2 using NH_3 as a reductant is considered to be an effective technology for the removal of NO_x from automotive emissions. The required ammonia is produced on board by decomposed and hydrolysis of stored urea in an additional tank.

Many catalysts have been reported to be active for SCR technology. The commercial catalyst for this process is V_2O_5/TiO_2 (anatase) promoted with either WO_3 or MoO_3 in stationary sources [3,6–9]. Although the vanadium-based catalyst is highly active and resistant to SO_2, many disadvantages of the catalyst still exist. The thermal stability of SCR catalyst is critical to withstand the harsh environment due to the high temperatures of the diesel exhaust during regeneration of diesel particulate filter (DPF), while the loss of activity of V_2O_5–WO_3/TiO_2 is unavoidable due to the phase change of TiO_2 from anatase to rutile around 600 °C. Furthermore, the toxicity of vanadium and the oxidation of SO_2 to SO_3 are drawbacks of the vanadium-based catalysts.

Transition metal supported on zeolite catalysts are promising alternative SCR catalysts for practical application in diesel engine, such as Fe-exchanged zeolite [10–14], and Fe containing oxide [15]. Especially, Fe-ZSM-5 was studied extensively in the past decade [16–20]. Although Fe-ZSM-5 seems to be one of the most effective catalysts used in the SCR reaction, the activity of SCR of NO_x at low temperature (<523 K) is still poor.

To improve the low temperature activity of SCR under lean burn conditions, many catalysts containing transition metal have been investigated for this reaction, such as V_2O_5/activated carbon [21,22], Mn-based metal oxides [23–26], etc. Our research group has prepared manganese and iron oxides supported on USY catalysts by impregnation. The catalysts have been investigated for the low temperature SCR of NO with NH_3, which can be operated in the low temperature range of 373–573 K. 10%Mn–8%Fe/USY has shown the most active in the range of 423–573 K. It was also investigated how the addition of Fe promoted the catalytic performance.

2. Experimental

2.1. Preparation of catalysts

The catalyst support was ultra-stable Y zeolite (USY, Si/Al = 5.2, Wenzhou Huahua Corporation). The catalyst was impregnated by

* Corresponding author. Tel.: +86 10 62771093; fax: +86 10 62771093.
E-mail address: lijunhua@tsinghua.edu.cn (J. Li).

0920-5861/$ – see front matter © 2010 Elsevier B.V. All rights reserved.
doi:10.1016/j.cattod.2010.01.026

incipient wetness with an aqueous solution of manganese acetate and/or iron nitrate. The impregnated sample was first dried at 393 K for 12 h, followed by calcination at 673 K in air for 6 h. The metal contents (wt%) of Mn and Fe are based on the support.

2.2. Characterization

N_2 adsorption was determined at 77 K on a NOVA4000 Micromeritics instrument. The samples were previously degassed at 523 K for 2 h. Specific surface areas were calculated by the BET method. For porosity analysis, the BJH method was used.

X-ray powder diffraction (XRD) patterns were measured with a Rigaku Model D/Max-RB and Ni-filtered Cu Kα radiation (λ = 1.5415 Å) was utilized in an X-ray tube operated at 40 kV and 100 mA.

X-ray photoelectron spectroscopy (XPS) test was carried on PHI-5300/ESCA. Using position sensitivity detector, Al/Mg double anode target, the energy resolution of 0.8 eV, sensitivity of 80 KCPS, an angular resolution of 45, and analysis chamber vacuum of 2.9×10^{-7} Pa. Sputtering conditions: Ar^+, scanning area of 8 mm × 8 mm, sputtering rate of 4 nm/min, energy of 3.0 kV, emission current of 25 mA.

Diffuse reflectance infrared Fourier transform spectroscopy (DRIFTS) was carried out on Nicolet Fourier transform infrared spectrometer with in situ diffuse reflectance pool and high-sensitivity MCT detector. Sampling resolution was 4 cm^{-1}, and scanning number was 100. Catalysts were placed directly in situ sample units within and compacted. Prior to experiment, the samples were purged in a flow of N_2 at 673 K for 60 min and then cooled to 303 K in a flow of N_2. At 303 K, the gas flow was switched to 500 ppm NH_3/N_2 or 500 ppm NO + 3% O_2/N_2 to adsorb NH_3 or NO for 60 min followed by purging with N_2 for 15 min. The total flow rate of all the test was 100 ml/min.

The FT-IR spectra of chemisorbed pyridine (Py-IR) were obtained on a Perkin-Elmer Model 2000 spectrophotometer in the 1750–1420 cm^{-1} range. The self-supported sample wafers were outgassed at 773 K for 1 h prior to pyridine adsorption. After the adsorption of pyridine at room temperature, the catalysts were outgassed at 373, 473, 573 and 673 K and their spectra were recorded.

2.3. Catalytic activity measurement

The activity measurement was carried out in a fixed-bed quartz reactor (inner diameter 8 mm) using a 0.5 g catalyst of 40–60 mesh. The reaction conditions were as follows: 500 ppm NO, 500 ppm NH_3, 3% O_2, 10% H_2O (when used), 100 ppm SO_2 (when used), balance N_2, 300 ml/min total flow rate. The NO and NO_2 concentrations were measured simultaneously by an on-line flue gas analyzer (KM9006 Quintox, Kane-May International Limited). The products were analyzed by a gas chromatograph (Shimadzu GC 17A) with a Parapak Q column for N_2O and a 5A molecular sieve column for N_2. All the data were obtained after 60 min when the SCR reaction reached steady state.

3. Results and discussion

3.1. Effect of Mn content of Mn/USY on SCR activity

Fig. 1 compares the NH_3-SCR activity of USY and Mn/USY with different Mn contents. In case of USY without manganese loading, the NO removal was negligible at all reaction temperatures, but adding manganese oxide enhanced the catalytic activity. It indicated that USY zeolite was inactive for the SCR of NO with NH_3, and Mn species must play a significant role in this catalytic reaction. With increasing Mn loading, NO conversion increased until it reached an optimum content of 10%. The conversion of NO to N_2 over 10% Mn/USY reached 98% in the temperature range from 453 to 543 K. Nevertheless, further increase of the Mn content the NO conversion decreased and the operation window narrowed.

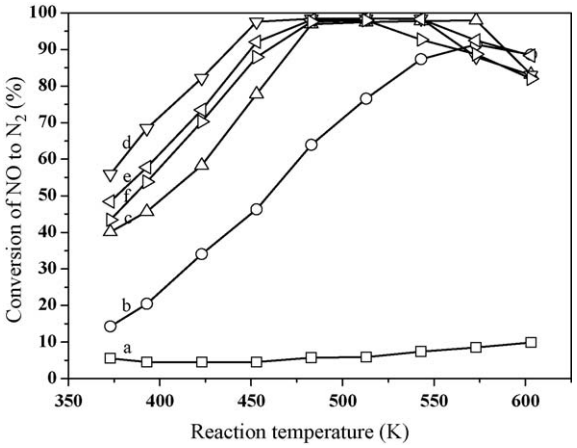

Fig. 1. Effect of manganese content on SCR activity of Mn/USY. (a) USY, (b) 4%Mn/USY, (c) 8%Mn/USY, (d) 10%Mn/USY, (e) 12%Mn/USY, (f) 15%Mn/USY. Reaction conditions: 0.5 g catalyst, 500 ppm NO, 500 ppm NH_3, 3% O_2, N_2 balance, GHSV = 36,000 h^{-1}.

3.2. Effect of Fe content of Mn–Fe/USY on SCR activity

10%Mn/USY catalyst showed good performance at high temperature. NO conversions obtained on 10%Mn–Fe/USY catalysts with different Fe loading at various temperatures were shown in Fig. 2. Compared with the activity of 10%Mn/USY catalyst, the addition of Fe to 10%Mn/USY enhanced the low temperature performance and widened the operating range of temperature. The 10%Mn–8%Fe/USY was the most active catalyst at low temperatures. At 373 K, the conversion of NO to N_2 over it reached 66.5%, and it obtained nearly 100% in the temperature range from 423 to 573 K. Among the catalysts, no N_2O production was detected at reaction temperatures below 483 K.

Baik et al. reported that Cu-ZSM5 catalyst revealed the highest performance of NO removal activity, particularly at low reaction temperatures below 250 °C, that is critical for the application to automotive diesel engines [27]. In our lab, we also prepared Cu-ZSM5 though ion-exchange method and tested its activity. The reaction condition was in line with 10%Mn–8%Fe/USY test. The results also showed that Cu-ZSM5 was highly active in the NO

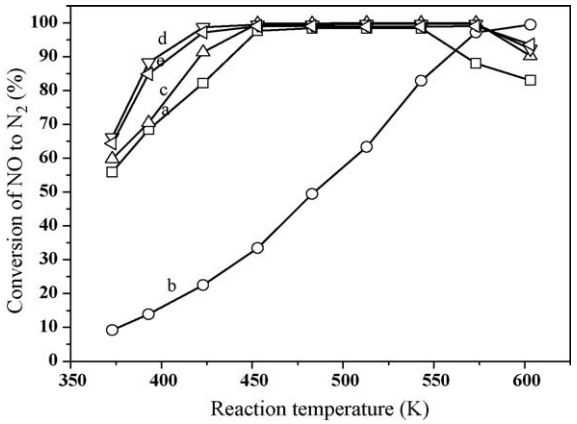

Fig. 2. Effect of iron content on SCR activity of Mn–Fe/USY. (a) 10%Mn/USY, (b) 10%Fe/USY, (c) 10%Mn–4%Fe/USY, (d) 10%Mn–8%Fe/USY, (e) 10%Mn–10%Fe/USY. Reaction conditions: 0.5 g catalyst, 500 ppm NO, 500 ppm NH_3, 3% O_2, N_2 balance, GHSV = 36,000 h^{-1}.

removal activity, which could reach about 100% NO conversions in the temperature range of 473–623 K. Compared to the results of Baik's and our tests, 10%Mn–8%Fe/USY might showed relatively higher NO conversion between 423 and 473 K. It should be noted that the catalytic activity of 10%Mn–8%Fe/USY could be inhibited by H_2O and SO_2 (refer to the following Section 3.3).

The present results addresses the practical evaluation of Mn–Fe/USY in the laboratory. Thus, we will do some researches about Mn–Fe/USY with particular focus on the diesel engines, and the hydrothermal and SO_2 aging of this catalyst would be studied systematically in the further experiment.

3.3. Effect of H_2O and SO_2 on SCR activity of Mn–Fe/USY

The emission of lean burn vehicles usually contains 10% water vapor, which also has a very significant impact on the catalytic activity of SCR. For most SCR catalyst, the presence of H_2O at low temperature reduces the $DeNO_x$ catalyst activity, while H_2O does not basically affect the NO_x conversion at higher temperature. We investigated the effect of 10% water vapor on catalytic activity of 10%Mn–8%Fe/USY at 423 K, and the results are shown in Fig. 3a. The results showed that the NO conversion gradually decreased and finally stabilized at around 78% due to the presence of 10% water vapor. When water vapor was removed from the reaction mixture, the catalytic activity has been rapidly recovered, the NO conversion recover to 95% after 1 h.

It is believed that the inhibition effect of H_2O on the catalytic activity of SCR is due to the competitive adsorption between H_2O and reactants (NH_3 and/or NO) on the active site for industrial catalysts V_2O_5/TiO_2 when the reaction temperature is lower than 623 K [28]. Topsøe et al. [29] found H_2O adsorption is weaker than the NH_3 adsorption on V_2O_5/TiO_2 catalyst surface. Therefore H_2O cannot inhibit the adsorption of NH_3, but enhanced much more Brönsted acid on the catalyst surface, which will increase the NH_3 adsorption. Low concentration of H_2O did not affect the adsorption–desorption balance of NH_3 on the V_2O_5–WO_3/TiO_2 catalyst surface, but significantly inhibited its SCR activity [30]. Considering water vapor effect on the catalytic activity of 10%Mn–8%Fe/USY, we believe that the inhibition may be due to the competitive adsorption of H_2O and the reactants (NH_3 and/or NO) on the active site.

Fig. 3b shows the result of 100 ppm SO_2 effects on catalytic activity. In the absence of SO_2, NO conversion can reach about 100% at 423 K. While in the presence of 100 ppm SO_2, the temperature window of active reaction shifts to the high temperature at 543 K, and the maximum NO conversion reaches over 90% between 573 and 653 K. This may be due to the sulfate species (such as $Fe_2(SO_4)_3$ or SO_4^{2-}/Fe_2O_3) deposited on catalyst surface, and catalytic active center was covered at low temperature. Long and Yang reported that Fe_2O_3 containing sulfate species were active in the ammonia oxidation reaction at 573–653 K, which might follow the same reaction mechanism of NH_3-SCR [31]. It is postulated that this kinds of species containing sulfates were highly active in the NH_3-SCR reaction and might increase reaction rate at 573–653 K. Therefore, the catalytic activity of 10%Mn–8%Fe/USY was not obviously influenced at high temperature.

Fig. 3c shows the activity results of 10%Mn–8%Fe/USY catalyst with coexistence of 10% H_2O and 100 ppm SO_2 at 453 K. It can be seen that NO conversion began to decline rapidly and eventually stabilized at around 60% as 10% H_2O and 100 ppm SO_2 were added to the reaction gas. After cutting off H_2O and SO_2, NO conversion was basically recovered and eventually stabilized at about 90%. We speculated that activity decline may be mainly due to the competitive adsorption of H_2O and SO_2 on the active site. But the existence of H_2O and SO_2 affected more slightly than SO_2 on the catalytic properties. To study the promotion effect of Fe, the catalysts were characterized by N_2 adsorption, XRD, XPS, DRIFTS and Py-IR.

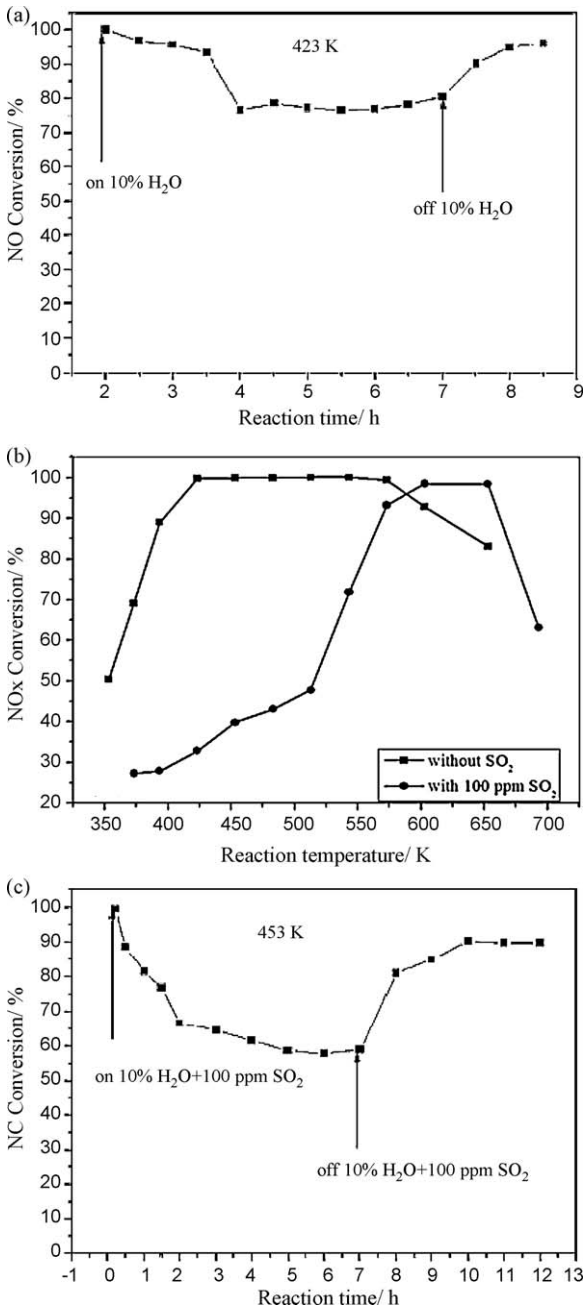

Fig. 3. Effect of H_2O and SO_2 on SCR activity of 10%Mn–8%Fe/USY. Reaction conditions: 0.5 g catalyst, 500 ppm NO, 500 ppm NH_3, 3% O_2, 10% H_2O (when used), 100 ppm SO_2 (when used), N_2 balance, GHSV = 36,000 h^{-1}.

3.4. N_2 adsorption

The BET data of USY and USY-supported catalysts calcined at different temperatures were summarized in Table 1. The surface area and pore volume of USY were 565 m^2/g and 0.3852 cm^3/g respectively. After doping with manganese oxide, the surface area and the pore volume of 10%Mn/USY decreased to 480 m^2/g and 0.3454 cm^3/g respectively. From Table 1, we can see that further doping iron oxide on 10%Mn/USY, the decrease of surface area and pore volume was not very severe. Furthermore, increasing the calcination temperature had little effect on the surface area and pore volume of 10%Mn/USY and 10%Mn–8%Fe/USY. The reason

Table 1
N_2 adsorption data of USY, Mn/USY, Fe/USY and Mn–Fe/USY.

Samples	Calcination temperature (K)	BET surface area (m^2/g)	Pore diameter (nm)	Pore volume (cm^3/g)
USY	673	565	2.728	0.3852
USY	873	554	2.715	0.3788
10%Mn/USY	673	480	2.873	0.3454
10%Mn/USY	873	475	2.821	0.3348
8%Fe/USY	673	425	2.936	0.3125
10%Mn–8%Fe/USY	673	433	2.857	0.3093
10%Mn–8%Fe/USY	873	431	2.798	0.3013

Table 2
XPS results of USY, 10%Mn/USY and 10%Mn–8%Fe/USY.

Sample	Al2p	Si2P	Mn2p		O1s	Fe2p	
			$Mn2p_{3/2}$	$Mn2p_{1/2}$		$Fe2p_{3/2}$	$Fe2p_{1/2}$
USY	74.6	102.7	/	/	532.0	/	/
10%Mn/USY	74.5	102.7	642.2	654.3	532.0	/	/
10%Mn–8%Fe/USY	74.4	102.6	641.8	653.6	529.9 532.0	711.2	724.9

that 10%Mn–8%Fe/USY increased the activity at low temperature may not be related to the surface area [32].

3.5. XRD

The XRD patterns of USY, Mn/USY with various Mn content, and 10%Mn–8%Fe/USY are shown in Fig. 4. It can be seen USY had several strong peaks, while after doping, the intensities of the peaks decreased. At low content (<10%), no visible manganese oxide phase can be observed. As the Mn loading increased, the crystal phase of MnO_2 appeared. No visible manganese or iron oxide phase was observed on 10%Mn–8%Fe/USY. This may be due to the weakly crystalline nature (amorphous) of the metal oxides. The coexistence of manganese and iron oxides enhanced the dispersion and lowered the crystallinity, which indicated that there were strong interactions between these two metal oxides [24,32].

3.6. XPS

Table 2 is the XPS results of USY, 10%Mn/USY and 10%Mn–8%Fe/USY. On the USY sample surface, the binding energy of Al, Si and O elements by XPS narrow scan was 74.6, 102.7 and 532.0 eV respectively. O1s binding at 529.5 ± 0.5 eV for the peak was usually identified as lattice oxygen O^{2-}, 531.0 ± 0.5 eV peak was identified as a single atom adsorbed oxygen O^-, and 532.6 ± 0.5 eV peak was identified as a molecule adsorbed oxygen O_2^{2-} [33]. Therefore, USY surface adsorbed oxygen species were mainly in O_2^{2-}form.

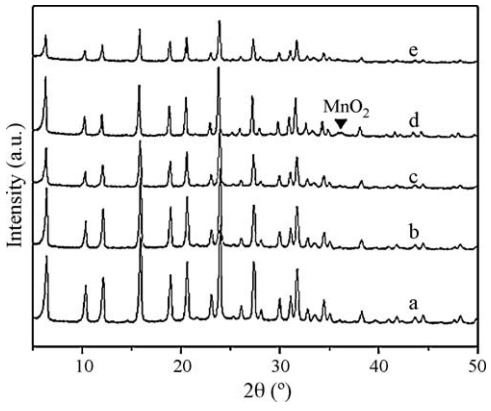

Fig. 4. XRD patterns of different samples. (a) USY, (b) 4%Mn/USY, (c) 10%Mn/USY, (d) 15%Mn/USY, (e) 10%Mn–8%Fe/USY.

Al2p, Si2p, and O1s peaks were also identified for Al, Si and O elements on 10%Mn/USY catalyst surface by XPS, and their binding energy was 74.5, 102.7 and 532.0 eV respectively. Compared to USY, the XPS results of 10%Mn/USY did not changed significantly. We speculated that surface oxygen species on 10%Mn/USY catalyst are still mainly adsorbed O_2^{2-} form. In the XRD spectra of 10%Mn/USY, no Mn oxide diffraction peaks was detected, which indicated Mn oxides was highly dispersed on the surface of USY. With the XPS results, it can be seen that the sample Mn2p3/2 binding energy was 642.2 eV. As reported in the literature [34,35], the binding energies of Mn_3O_4, Mn_2O_3 and MnO_2 were respectively at 641.3–641.4, 641.3–641.7, and 641.7–642.2 eV. Therefore, Mn species on 10%Mn/USY catalyst surface were mainly in the form of MnO_2.

Al2p and Si2p peaks were also collected on 10%Mn–8%Fe/USY catalyst surface in a narrow scan, and their binding energy was at 74.4 and 102.7 eV respectively. Compared to XPS results of 10%Mn/USY catalyst, binding energy did not change significantly. From O1s peak analysis of 10%Mn–8%Fe/USY catalyst, we found that the O1s peak changed significantly compared to 10%Mn/USY catalyst, which split into two peaks and formed shoulder shaped peak in the low binding energy. The peaks can be decomposed into two peaks of low binding energy at 529.9 eV and the higher binding energy at 532.0 eV. Therefore, Fe additive resulted in a large number of lattice oxygen. Compared with surface adsorbed oxygen species, lattice oxygen or oxygen vacancy might have higher activity at low temperature in the NH_3-SCR reaction[25], which was more likely to oxidized NO to NO_2 on the catalyst surface to form a monodentate and bidentate nitrate species, thus contributing to the activity of catalyst.

Mn2p3/2, binding energy of 10%Mn–8%Fe/USY at 641.8 eV, showed Mn species still existed in the MnO_2 form. But as compared with 10%Mn/USY, Mn2p3/2 binding energy showed a decrease about 0.4 eV. This may be due to a strong interaction between Mn and Fe. Fe addition made the Mn and Fe central part of charge shift, resulted in the increasing of Mn outer electron cloud density, and shielding effect enhanced. This effect might make the valence of Mn atoms decrease. Due to reduction of Mn2p3/2 binding energy caused by the mutual synergies of Mn and Fe, activation energy become lower, the reaction becomes easier. Therefore, Fe additives caused lattice oxygen formation and Mn2p3/2 binding energy reduction.

According to the XRD spectra of 10%Mn–8%Fe/USY catalyst, we did not detect any Fe oxide diffraction peaks in addition to USY diffraction peaks. In order to obtain Fe valence state of 10%Mn–8%Fe/USY catalyst, we scanned its narrow Fe2p peak. The results

showed that Fe2p3/2 binding energy was at 711.2 eV. Considering O1s peak appears at 529.9 eV, we can speculate Fe species was in the form of γ-Fe_2O_3.

Based on XPS studies, Mn and Fe oxides on 10%Mn–8%Fe/USY catalyst, which were prepared by impregnation, were mainly formed MnO_2 and γ-Fe_2O_3. Due to the strong synergy between Mn and Fe, Mn2p3/2 binding energy reduced about 0.4 eV. Besides surface adsorbed oxygen species, there was a large number of lattice oxygen to form. Both of the combined effect improved $DeNO_x$ activity of the 10%Mn–8%Fe/USY catalyst.

3.7. DRIFTS

Fig. 5a shows the DRIFTS spectra of 10%Mn/USY and 10%Mn–8%Fe/USY catalyst adsorption with 500 ppm NO + 3% O_2/N_2 after 60 min. As can be seen, the absorption peaks on different samples are observed at 1150, 1309, 1512 and 1639 cm^{-1}. 1309 and 1512 cm^{-1} were strong absorption peaks, while the 1150 and 1639 cm^{-1} absorption peaks were weak. 1147 and 1631 cm^{-1} absorption peaks were corresponded to NO adsorption species, and 1147 cm^{-1} for monodentate nitrite symmetric stretching vibration, 1631 cm^{-1} for the weak adsorption of gas phase NO or NO_2. 1315 and 1505 cm^{-1} were corresponded to the NO_2 species absorption peak, and 1315 cm^{-1} for bidentate nitrate stretching vibration, 1505 cm^{-1} for the stretching vibration of monodentate nitrate [36–38]. DRIFTS results showed that NO_x on 10%Mn/USY and 10%Mn–8%Fe/USY catalyst surface are mainly monodentate and bidentate nitrate. As compared with 10%Mn/USY catalyst, Fe addition clearly enhanced 1309 and 1512 cm^{-1} absorption peaks, which indicated Fe promoted NO oxidation and create more monodentate and bidentate nitrates adsorbed species on the catalyst surface. The species, which were easier to be reduced by NH_3 active species, probably enhanced higher activity.

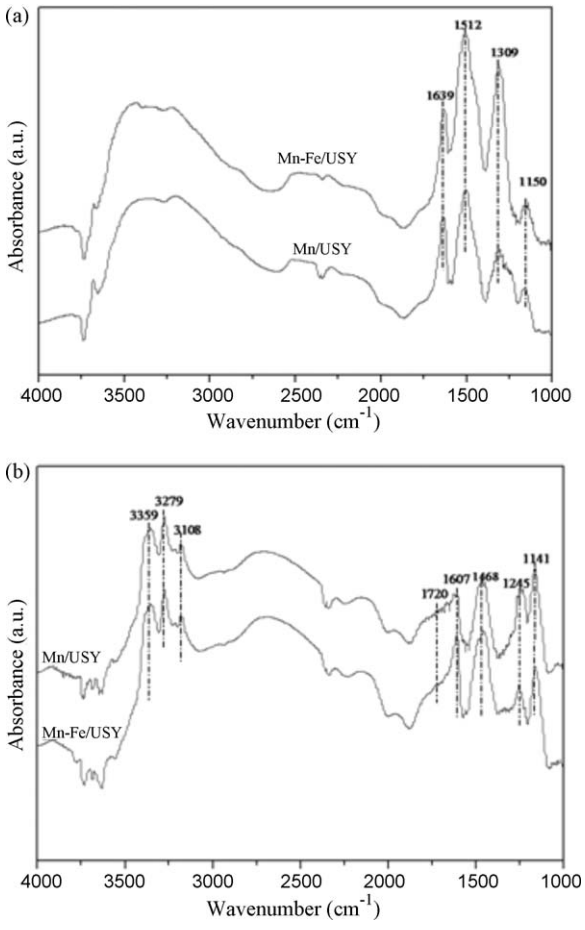

Fig. 5. (a) DRIFTS spectra of NO + O_2 adsorbed on the catalysts and (b) DRIFTS spectra of NH_3 adsorbed on the catalysts.

Fig. 5b shows the NH_3 saturated adsorption DRIFTS spectra of 10%Mn/USY and 10%Mn–8%Fe/USY catalyst. As can be seen, the absorption peak appeared at 3359, 3279, 1720, 1607, 1468, 1245 and 1141 cm^{-1} on different samples. 1720 and 1468 cm^{-1} were ascribed to NH_4^+ symmetric and asymmetric stretching vibration of chemical adsorption on the Brönsted acid sites. 1607, 1245 and 1141 cm^{-1} were NH symmetric and asymmetric stretching vibration of NH_3 molecules coordinating with the Lewis acid sites. 3372 and 3276 cm^{-1} were symmetric and asymmetric stretching vibration of NH_3 on Lewis acid sites [36–38]. DRIFTS results showed that NH_3 was mainly chemical adsorption of NH_4^+ on Brönsted acid sites and coordinated NH_3 on Lewis acid sites on 10%Mn/USY and 10%Mn–8%Fe/USY catalyst surface. As compared with 10%Mn/USY catalyst, we speculated that Fe addition made 1720, 1468 and 1607 cm^{-1} absorption peaks become strong, while made the 1245 cm^{-1} absorption peak apparently weak. The analysis showed Fe promoted the adsorption activity of NH_3 on the Brönsted acid sites and formed more NH_4^+, which have higher activity than the coordinated combination of NH_3 species on Lewis acid sites. This may be another reason that Fe additive improved $DeNO_x$ activity.

3.8. Py-IR

The spectra of pyridine adsorbed on 10%Mn/USY and 10%Mn–8%Fe/USY after outgassing at different temperatures are shown in Fig. 6. All the spectra were normalized and recorded under identical operating conditions. The results indicated that all samples evacuated at 373 K after pyridine adsorption exhibited IR bands at about 1450, 1490, 1545, and 1604 cm^{-1}. The bands at 1450 and 1604 cm^{-1} are commonly assigned to Lewis acid sites, the band at 1490 cm^{-1} is mainly attributed to Lewis and Brönsted acid sites, and the band at 1545 cm^{-1} is due to Brönsted acid sites [39,40]. Both the Lewis and the Brönsted acid centers were found on the surfaces of the catalysts, and they declined gradually with increasing evacuation temperatures. By a comparison of the catalysts, for 10%Mn/USY, the bands at 1490 and 1541 cm^{-1} completely disappeared after evacuation at 673 K. However, for 10%Mn–8%Fe/USY, the outstanding feature was the increase in the number and strength of the Brönsted (1541 and 1489 cm^{-1}) and Lewis (1489 cm^{-1}) acid centers. After the evacuation at 373 K, the bands at 1541 and 1489 cm^{-1} were somewhat more intense than those on 10%Mn/USY, and still existed for evacuating at 673 K although a significant loss of intensity was observed for 10%Mn/USY.

Ammonia molecules are adsorbed on Brönsted and Lewis acid centers of the catalyst to generate respectively NH_4^+ ions and coordinated NH_3 species, which could react with NO_x adspecies to form active complexes $NO_2[NH_4^+]_2$ and $NO_2[NH_3]_2$. The improvement of surface acidity will increase the concentration of ammonia adsorption and thus enhance the amount of NH_3 and NH_4^+ pair, which will also increase the catalytic activity for the SCR reaction [36]. Fe promotion effect in 10%Mn/USY for low temperature SCR of NO with NH_3 might be due to the increase in the number of the Brönsted and Lewis acid centers.

The maximum of Lewis and Brönsted acid centers along with recording the spectra under actual reaction conditions can identify the surface characteristics necessary for operation at low temperatures. An exhaustive study describing the adsorption–desorption characteristics of the gases, such as, NH_3, NO, O_2, or the mixture of the two or more gases on 10%Mn/USY or 10%Mn–8%Fe/USY by in situ FT-IR will be thoroughly investigated in our following research work and reported in the subsequent paper.

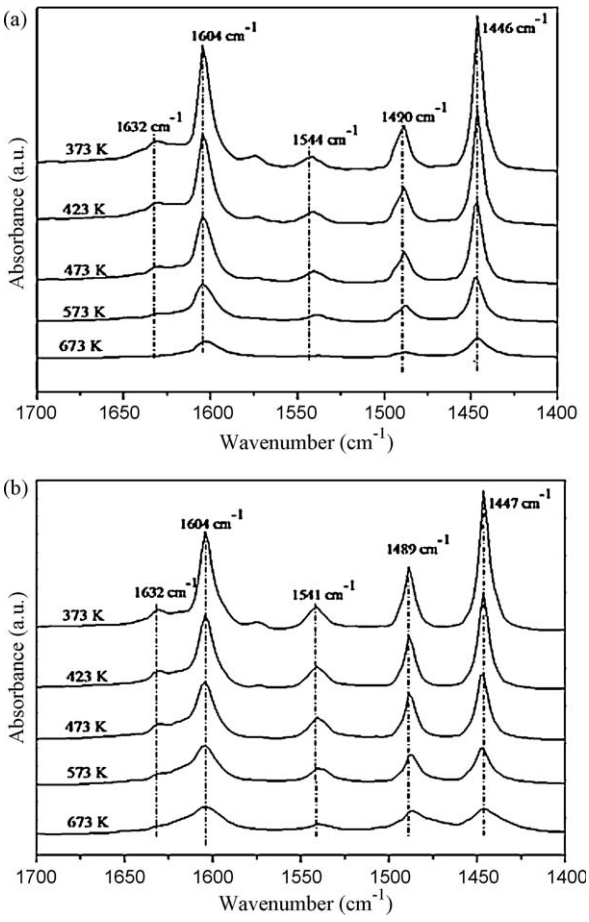

Fig. 6. IR spectra of pyridine adsorbed on the catalysts. (a) 10%Mn/USY and (b) 10%Mn–8%Fe/USY.

4. Conclusion

10%Mn–8%Fe/USY showed highly active for the low temperature SCR of NO with NH_3 in the presence of excess oxygen. Nearly 100% NO conversion on the catalyst was obtained at 423 K at a space velocity of 36,000 h^{-1}, and no N_2O was detected when the temperature was below 483 K. But H_2O and SO_2 had strong impact on SCR activity of 10%Mn–8%Fe/USY at low temperature because of the competitive adsorption of H_2O and SO_2 on the active site. Mn and Fe oxides on 10%Mn–8%Fe/USY catalyst, which were prepared by impregnation, were mainly formed MnO_2 and γ-Fe_2O_3. The promotion effect of Fe might be due to the enhancement of the dispersion of manganese and iron oxides on USY, the acidity on the catalyst surface and NO oxidation, all of which were critical role in the NH_3-SCR reaction.

Acknowledgements

This work was supported by National Natural Science fund of China (Grant No. 20677034), National High Science & Technology Project (863, Grant No. 2009AA064806) and Ford Motor Company.

References

[1] H. Bosch, F. Janssen, Catal. Today 2 (1988) (v).
[2] M. Shelef, Chem. Rev. 95 (1995) 209.
[3] G. Busca, L. Lietti, G. Ramis, F. Berti, Appl. Catal. B 18 (1998) 1.
[4] V.I. Parvulescu, P. Grange, B. Delmon, Catal. Today 46 (1998) 233.
[5] N. Jagtap, S.B. Umbarkar, P. Miquel, P. Granger, M.K. Dongare, Appl. Catal. B 90 (2009) 416.
[6] R.M. Heck, Catal. Today 53 (1999) 519.
[7] P.H. Mutin, A.F. Popa, A. Vioux, G. Delahay, B. Coq, Appl. Catal. B 69 (2006) 49.
[8] H.H. Phil, M.P. Reddy, P.A. Kumar, L.K. Ju, J.S. Hyo, Appl. Catal. B 78 (2008) 301.
[9] X. Zhang, X.G. Li, J.S. Wu, R.C. Yang, Z.H. Zhang, Catal. Lett. 130 (2009) 235.
[10] P. Gilot, M. Guyon, B.R. Stanmore, Fuel 76 (1997) 507.
[11] R.Q. Long, R.T. Yang, J. Am. Chem. Soc. 121 (1999) 5595.
[12] A.Z. Ma, W. Grunert, Chem. Commun. (1999) 71.
[13] S. Brandenberger, O. Krocher, A. Tissler, R. Althoff, Catal. Rev.-Sci. Eng. 50 (2008) 492.
[14] A. Grossale, I. Nova, E. Tronconi, Catal. Today 136 (2008) 18.
[15] N. Apostolescu, B. Geiger, K. Hizbullah, M.T. Jan, S. Kureti, D. Reichert, F. Schott, W. Weisweiler, Appl. Catal. B 62 (2006) 104.
[16] M. Iwasaki, K. Yamazaki, K. Banno, H. Shinjoh, J. Catal. 260 (2008) 205.
[17] O. Krocher, M. Devadas, M. Elsener, A. Wokaun, N. Soger, M. Pfeifer, Y. Demel, L. Mussmann, Appl. Catal. B 66 (2006) 208.
[18] K. Krishna, M. Makkee, Catal. Today 114 (2006) 23.
[19] M. Schwidder, W. Grunert, U. Bentrup, A. Bruckner, J. Catal. 239 (2006) 173.
[20] M. Schwidder, M.S. Kumar, K. Klementiev, M.M. Pohl, A. Bruckner, W. Grunert, J. Catal. 231 (2005) 314.
[21] Z.G. Huang, Z.P. Zhu, Z.Y. Liu, Appl. Catal. B 39 (2002) 361.
[22] Z.G. Huang, Z.P. Zhu, Z.Y. Liu, Q.Y. Liu, J. Catal. 214 (2003) 213.
[23] Z.B. Wu, R.B. Jin, H.Q. Wang, Y. Liu, Catal. Commun. 10 (2009) 935.
[24] G.S. Qi, R.T. Yang, Appl. Catal. B 44 (2003) 217.
[25] G.S. Qi, R.T. Yang, J. Phys. Chem. B 108 (2004) 15738.
[26] M. Richter, A. Trunschke, U. Bentrup, K.W. Brzezinka, E. Schreier, M. Schneider, M.M. Pohl, R. Fricke, J. Catal. 206 (2002) 98.
[27] J.H. Baik, S.D. Yim, I.S. Nam, Y.S. Mok, J.H. Lee, B.K. Cho, S.H. Oh, Top. Catal. 30/31 (2004) 37.
[28] M.D. Amiridis, I.E. Wachs, G. Deo, J.M. Jehng, D.S. Kim, J. Catal. 161 (1996) 247.
[29] N.Y. Topsøe, T. Slabiak, B.S. Clausen, T.Z. Srnak, J.A. Dumesic, J. Catal. 134 (1992) 742.
[30] I. Nova, L. Lietti, E. Tronconi, P. Forzatti, Catal. Today 60 (2000) 73.
[31] R.Q. Long, R.T. Yang, J. Catal. 207 (2002) 158.
[32] G.S. Qi, R.T. Yang, R. Chang, Catal. Lett. 87 (2003) 67.
[33] X. Yang, S. Liu, X. Ye, Y. Wu, Acta Phys. Chim. Sin. 11 (1995).
[34] M.C. Alvarez-Galvan, B. Pawelec, V.A.D. O'Shea, J.L.G. Fierro, P.L. Arias, Appl. Catal. B 51 (2004) 83.
[35] D.A. Pena, B.S. Uphade, P.G. Smirniotis, J. Catal. 221 (2004) 421.
[36] R.Q. Long, R.T. Yang, J. Catal. 190 (2000) 22.
[37] R.Q. Long, R.T. Yang, J. Catal. 207 (2002) 224.
[38] V. Sanchez-Escribano, T. Montanari, G. Busca, Appl. Catal. B 58 (2005) 19.
[39] J.A. Lercher, C. Grundling, G. EderMirth, Catal. Today 27 (1996) 353.
[40] K.T.D. Roseno, M.A.S. Baldanza, M. Schmal, Catal. Lett. 124 (2008) 59.